buildings

MDPI

Article

Grid Optimization of Free-Form Spatial Structures Considering the Mechanical Properties

Fengcheng Liu [1,*], Tao Xu [1], Yung William Sasy Chan [1] and Konstantinos Daniel Tsavdaridis [2]

[1] College of Architectural Science and Engineering, Yangzhou University, Yangzhou 225127, China; sasychanwill@yahoo.com (Y.W.S.C.)
[2] Department of Engineering, School of Science and Technology, City, University of London, London EC1V 0HB, UK
* Correspondence: lfc110@163.com

Abstract: In recent years, the application of free-form surface spatial grid structures in large public buildings has become increasingly common. The layouts of grids are important factors that affect both the mechanical performance and aesthetic appeal of such structures. To achieve a triangular grid with good mechanical performance and uniformity on free-form surfaces, this study proposes a new method called the "strain energy gradient optimization method". The grid topology is optimized to maximize the overall stiffness, by analyzing the sensitivity of nodal coordinates to the overall strain energy. The results indicate that the overall strain energy of the optimized grid has decreased, indicating an improvement in the structural stiffness. Specifically, compared to the initial grid, the optimized grid has a 30% decrease in strain energy and a 43.3% decrease in maximum nodal displacement. To optimize the smoothness of the grid, the study further applies the Laplacian grid smoothing method. Compared to the mechanically adjusted grid, the structural mechanical performance does not significantly change after smoothing, while the geometric indicators are noticeably improved, with smoother lines and regular shapes. On the other hand, compared to the initial grid, the smoothed grid has a 21.4% decrease in strain energy and a 28.3% decrease in maximum nodal displacement.

Keywords: free-form surface; spatial grid structure; grid layout; strain energy gradient; grid optimization

Citation: Liu, F.; Xu, T.; Chan, Y.W.S.; Tsavdaridis, K.D. Grid Optimization of Free-Form Spatial Structures Considering the Mechanical Properties. *Buildings* **2024**, *14*, 3191. https://doi.org/10.3390/buildings14103191

Academic Editor: Annalisa Greco

Received: 10 September 2024
Revised: 21 September 2024
Accepted: 24 September 2024
Published: 7 October 2024

1. Introduction

Free-form surface spatial grid structure, as the name implies, includes two parts: surface and grid. The freedom of the curved surface form highlights its elegant and lively shape and interprets the beauty of the building, while the grid is its skeleton part, and its architectural charm is finally reflected through a reasonable grid layout.

The grid division of free-form surfaces needs to consider the uniformity and smoothness of the architectural grid, as well as the regularity of grid shapes. Generally, the methods for dividing grids on free-form surfaces can be broadly classified into two types: one is the indirect grid division method based on the principles of traditional mapping method; the other is a direct grid partition method that directly takes the building surface as the operating object and generates the surface grid through different optimization algorithms.

The mapping method is one of the most widely used indirect grid generation techniques in the current application of free-form surface spatial grid structures. It has the advantages of simple principles, ease of implementation, high efficiency, and strong grid controllability [1]. Based on the mapping method, Cen [2] proposed an approximate arc-length parameterization method, utilizing bicubic B-spline interpolation on curved surface value points (original data points) to reconstruct free-form surfaces to avoid the mapping distortion caused by traditional mapping methods. Based on the tensor product characteristics of the B-spline surface, Ding [3] proposed an isoparametric line segmentation method for free-form reticulated shell structures. Wei et al. [4], combining the principles of the traditional mapping method and surface equal area expansion technology, established a bi-directional mapping relationship between spatial

surfaces and planes, which reduces the errors caused by mapping [5,6]. Cuilliere et al. [7] established a mapping metric mechanism based on the consideration of grid mapping deformation, proposed a meshing method suitable for free-form surfaces, and proposed an evaluation index of grid quality. Zheleznyakova et al. [8,9] proposed a quasi-molecular motion method based on a mapping technique and physical simulation method, which can adjust the size of the plane grid according to the difference of intermolecular forces, so as to reduce the grid distortion after mapping back to the space surface.

The direct grid generation techniques can be roughly summarized into the following methods: surface subdivision algorithms [10–12], compass method, physics analogical methods (such as bubble method), surface stress line method, and so on. Lina and Lefevre [13,14] developed a compass grid generation method to obtain uniform quadrilateral grids on free-form surfaces, which can generate curved quadrilateral grids on surfaces with completely equal rod lengths. Shimada and Zhou [15,16] analogized the grid division of parameterized surfaces to finding equilibrium positions in densely packed bubbles and proposed the bubble packing method.

Wang et al. [17] referred to the bubble generation method and directly generated bubbles on the space surface to avoid mapping distortion, which is called the space bubble method. Similarly, Pottmann et al. [18] developed the CP-mesh method (circle packing method) suitable for spatial surfaces based on the tangential relationship between spheres on surfaces. This method can generate joints without twisting and has been extensively applied in curtain wall structures. Based on the advancing front method, Su [19] proposed an improved advancing front method aimed at improving the mechanical performance of grids, which takes the structural stress trajectory line as the guideline to make the grid advance in the direction of the guideline, avoiding blindness and disorder of grid propulsion.

Using the above methods, architectural grids with smooth lines, uniform rod length, and rich styles can be obtained, but most of the research still stays at the geometric level and does not investigate the final structural mechanical properties [20]. Zhang [21] proposed a polygon mesh partitioning method and a mesh optimization method based on force, further enriching the content of free-form surface mesh design. Actually, for the free-form surface spatial grid structure, the topological form of the grid often affects the mechanical properties of the structure more than the material and component size [22]. The distribution of the joint position and the topological form of the bar not only highlight the architectural beauty of the structure but also bear the soul of structural stress, which is an important factor affecting the bearing capacity of the spatial grid structure. Therefore, it is necessary to study the grid optimization method based on the mechanical properties of the structure.

To seek a layout of structural elements with superior mechanical properties within predetermined constraints of architectural surfaces, it is necessary to optimize the surface according to its stress characteristics. In order to obtain a grid arrangement with both good mechanical properties and smooth lines on free-form surfaces, this paper proposes a new method called the "strain energy gradient optimization method" based on the sensitivity of strain energy to the change of the nodal coordinates. With the overall strain energy of the structure as the objective and the free-form surface as the constraint, the gradient of strain energy on nodal coordinates is derived, and then the grid optimization is carried out to obtain the grid topology with the highest stiffness.

2. Strain Energy Gradient and Joint Adjustment Strategy

In the morphological optimization of spatial grid structures on free-form surfaces, the structural strain energy is often chosen as the objective to attain a structure with higher rigidity [23]. Similarly, when seeking a grid layout with increased rigidity under given surface constraints, the structural strain energy can also be used as the objective function. If the overall structural strain energy is viewed as a function $C(X)$ of grid nodal coordinates, the task of seeking a reasonable grid layout on a given surface becomes an optimization problem of minimizing the strain energy $C(X)$. The optimization mathematical model can be expressed as $minC(X)$. In the formula, X represents the set of nodal coordinates. As the

exploration involves seeking a rational grid layout on a predefined surface, the structural form remains unchanged throughout the optimization process. Therefore, in this study, vertical changes in nodal coordinates (the z-direction) are neglected, considering only the movement of joints along the x and y directions.

The fundamental approach for node adjustment can be summarized as follows: First, the initial structural details, including information about the spatial surface, initial nodal coordinates, initial topological connections between nodes, loadings, and support nodes information, are provided. Second, a finite element analysis is conducted on the initial structure to obtain nodal displacements, internal forces in members, and other relevant data. The circular steel tube with a diameter of 100 mm and a thickness of 4 mm was used, with Young's modulus and yield strength of 2.06×10^5 and 345 MPa, respectively. Subject to a dead load and a distributed live load, the strain energy gradient of the structure is calculated and nodal positions are adjusted aiming to minimize strain energy, updating relevant information after structural changes. Finally, it is assessed whether the updated structure meets the convergence criteria; if so, the optimization proceeds. If not, repeating the process of structural analysis, nodal position adjustment, and updating structural topological information until convergence criteria are met or the specified iteration limit is reached.

Assuming the set of grid nodal coordinates $\{X\}$ as the sole influencing factor on the structural strain energy, if the number of joints in the spatial grid structure is N and the structural strain energy is a function of nodal coordinates, denoted as $C(X)$, its Taylor expansion at joint X is expressed as shown in Formula (2):

$$C(X + \Delta X_i) = C(X) + \sum_{i=1}^{N} \frac{\partial C(X)}{\partial X_i} \Delta X_i + \phi \tag{1}$$

In the formula, ϕ represents a higher-order infinitesimal, which is disregarded and omitted here. By introducing an adjustment step size λ, the change in nodal coordinates can be expressed as follows:

$$\Delta X_i = -\lambda \frac{\partial C(X)}{\partial X_i} = -\lambda \alpha_i \tag{2}$$

α_i represents the strain energy gradient. Then, Formula (1) can be written as follows:

$$C(X + \Delta X_i) = C(X) - \lambda \sum_{i=1}^{N} \left(\frac{\partial C(X)}{\partial X_i}\right)^2 = C(X) - \lambda \sum_{i=1}^{N} \alpha_i^2 \leq C(X) \tag{3}$$

By adjusting the node coordinates according to Formula (3), the structural strain energy will gradually decrease after the node coordinates change, and a reasonable grid layout scheme with smaller structural strain energy will be obtained. If α_i equals zero, it indicates that the strain energy has reached its minimum value. At this point, the change in strain energy is independent of the change in node coordinates and remains unchanged. However, this scenario is rather ideal and is often challenging to achieve. To attain a grid layout with lower strain energy, the nodal coordinate adjustment strategy can be implemented as outlined in Formula (4).

$$P_i^{k+1} = P_i^k - \lambda \alpha_i^k \tag{4}$$

In the formula, P_i^{k+1} represents the coordinates of joint i at the (k+1)th step. α_i^k stands for the strain energy gradient of the ith joint in the structure at the kth step, also serving as the direction for joint updates. Actually, updating the nodal coordinates in the direction of the negative gradient is the fastest way to decrease structural strain energy. λ denotes the adjustment step size, which is an empirical parameter. If set too large, it may fail to meet the requirement in Formula (3); if set too small, it may reduce the optimization efficiency. Typically, a value around $1/(5\alpha_{\max}^0)$ is advisable.

2.1. The Derivation of the Strain Energy Gradient

The strain energy gradient can also be referred to as strain energy sensitivity, which illustrates how the overall structural strain energy changes with variations in design

variables. As shown in Formula (5), the gradient of structural strain energy at joint *i* can be expressed as follows:

$$\alpha_i = \frac{\partial C(X_i)}{\partial X_i} \tag{5}$$

The general derivation process is briefly introduced as follows. Firstly, under external loading, the fundamental finite element formulas for the spatial grid structure on free-form surfaces can be expressed as follows:

$$K(X)U(X) = P(X) \tag{6}$$

The formula components include K as the total stiffness matrix of the spatial grid structure; U as the total displacement vector matrix of the grid structure; P as the vector representing the applied nodal loads on the grid structure; and X as the collection of nodal coordinates for the grid structure. The overall strain energy of the grid structure can be represented as follows:

$$C(X) = \frac{1}{2}P(X)^T U(X) \tag{7}$$

The differentiation of the structural joint coordinate components in Formulas (6) and (7) leads to the following two formulas:

$$\frac{\partial C}{\partial x} = \frac{1}{2}P^T \frac{\partial U}{\partial x} \tag{8}$$

$$\frac{\partial K}{\partial x}U + K\frac{\partial U}{\partial x} = 0 \tag{9}$$

Next, by simply integrating Formulas (8) and (9), we arrive at the strain energy gradient with respect to the nodal x-direction coordinate, as illustrated in Formula (10).

$$\frac{\partial C}{\partial x} = -\frac{1}{2}U^T \frac{\partial K}{\partial x}U \tag{10}$$

The similar strain energy gradients with respect to the y- and z-direction coordinates can be expressed as follows:

$$\frac{\partial C}{\partial y} = -\frac{1}{2}U^T \frac{\partial K}{\partial y}U \tag{11}$$

$$\frac{\partial C}{\partial z} = -\frac{1}{2}U^T \frac{\partial K}{\partial z}U \tag{12}$$

2.2. The Differentiation of the Element Stiffness Matrix in the Local Coordinate System

This paper illustrates the derivation process of the differential of the beam element stiffness matrix with respect to nodal coordinates, using a planar structure as an example. For the one-dimensional planar beam element, as depicted in Figure 1, the global coordinate system is xyz, where the x and y axes lie within the plane of the beam element and the z-axis is perpendicular to the element plane. The global coordinate system intersects with the local coordinate system x*y* at an α angle. Then, the element stiffness matrix for beam element i in the local coordinate system is expressed as Formula (13).

$$k_i^{*e} = \begin{bmatrix} \frac{E_iA_i}{l_i} & 0 & 0 & -\frac{E_iA_i}{l_i} & 0 & 0 \\ 0 & \frac{12E_iI_i}{{l_i}^3} & \frac{6E_iI_i}{{l_i}^2} & 0 & -\frac{12E_iI_i}{{l_i}^3} & \frac{6E_iI_i}{{l_i}^2} \\ 0 & \frac{6E_iI_i}{{l_i}^2} & \frac{4E_iI_i}{l_i} & 0 & -\frac{6E_iI_i}{{l_i}^2} & \frac{2E_iI_i}{l_i} \\ -\frac{E_iA_i}{l_i} & 0 & -\frac{6E_iI_i}{{l_i}^2} & \frac{E_iA_i}{l_i} & 0 & 0 \\ 0 & -\frac{12E_iI_i}{{l_i}^3} & -\frac{6E_iI_i}{{l_i}^2} & 0 & \frac{12E_iI_i}{{l_i}^3} & -\frac{6E_iI_i}{{l_i}^2} \\ 0 & \frac{6E_iI_i}{{l_i}^2} & \frac{2E_iI_i}{l_i} & 0 & -\frac{6E_iI_i}{{l_i}^2} & \frac{4E_iI_i}{l_i} \end{bmatrix} \tag{13}$$

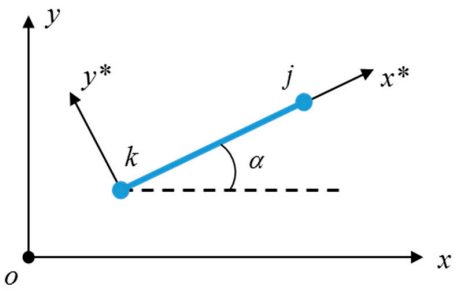

Figure 1. Global and local coordinate systems.

In the formula, E_i, A_i, I_i, and l_i, respectively, represent the material's elastic modulus, cross-sectional area, moment of inertia, and the geometric length of the element i. From Formula (13), it is evident that when the section of the rod remains unchanged, the stiffness matrix of element i in the local coordinate system is solely a function of the element length l, which is related to the coordinates of its two end joints. If the two end joints of element i are denoted as k and j, the element length can be expressed as follows:

$$l_i = \sqrt{(x_j - x_k)^2 + (y_j - y_k)^2} \tag{14}$$

Next, in the above Formula (14), the two end joints j and k of element i, respectively, are differentiated. And the j end is differentiated firstly, as shown in Formula (15).

$$dl_i = \frac{x_j - x_k}{l_i} dx_j + \frac{y_j - y_k}{l_i} dy_j \tag{15}$$

The expression for the differentiation of the element length with respect to the j end can be obtained.

$$\frac{dl_i}{dx_j} = \frac{x_j - x_k}{l_i} \tag{16}$$

$$\frac{dl_i}{dy_j} = \frac{y_j - y_k}{l_i} \tag{17}$$

Then, the corresponding differential expression is obtained by deriving the k-terminal derivative.

$$\frac{dl_i}{dx_k} = \frac{x_k - x_j}{l_i} \tag{18}$$

$$\frac{dl_i}{dy_k} = \frac{y_k - y_j}{l_i} \tag{19}$$

Thus, according to the chain rule of differentiation, the differential of the stiffness matrix of structural element i concerning changes in the coordinates of element m in the local coordinate system is derived, as shown in Formulas (20) and (21). In Formula (20), the parameter γ represents the position-related parameter within the rod element unit, indicating whether the joint is located at the beginning or end of the element. If the joint is at the end of the rod element, it takes the value $\gamma = (x_j - x_k)/l_i$; if it is at the beginning, it takes the value $\gamma = -(x_j - x_k)/l_i$. Similarly, if differentiating with respect to the joint's y-coordinate, it is only necessary to replace the variable x with y in γ.

$$\frac{\partial k_i^{*e}}{\partial x_m} = \begin{bmatrix} -\gamma\frac{E_iA_i}{l_i^2} & 0 & 0 & \gamma\frac{E_iA_i}{l_i^2} & 0 & 0 \\ 0 & -\frac{36\gamma E_iI_i}{l_i^4} & -\frac{12\gamma E_iI_i}{l_i^3} & 0 & \frac{36\gamma E_iI_i}{l_i^4} & \frac{12\gamma E_iI_i}{l_i^3} \\ 0 & -\frac{12\gamma E_iI_i}{l_i^3} & -\frac{4\gamma E_iI_i}{l_i^2} & 0 & \frac{12\gamma E_iI_i}{l_i^3} & -\frac{2\gamma E_iI_i}{l_i^2} \\ \gamma\frac{E_iA_i}{l_i^2} & 0 & 0 & -\gamma\frac{E_iA_i}{l_i^2} & 0 & 0 \\ 0 & \frac{36\gamma E_iI_i}{l_i^4} & \frac{12\gamma E_iI_i}{l_i^3} & 0 & -\frac{36\gamma E_iI_i}{l_i^4} & \frac{12\gamma E_iI_i}{l_i^3} \\ 0 & \frac{12\gamma E_iI_i}{l_i^3} & -\frac{2\gamma E_iI_i}{l_i^2} & 0 & \frac{12\gamma E_iI_i}{l_i^3} & -\frac{4\gamma E_iI_i}{l_i^2} \end{bmatrix} (i = m) \tag{20}$$

Or

$$\frac{\partial k_i^{*e}}{\partial x_m} = 0 \ (i \neq m) \tag{21}$$

2.3. The Differentiation of the Coordinate Transformation Matrix

In the global coordinate system, there exists a relationship between the stiffness matrix k_i^e of beam element i and the stiffness matrix k_i^{*e} in the local coordinate system, as illustrated in Formula (22).

$$k_i^e = R^T k_i^{*e} R \tag{22}$$

The symbol R represents the coordinate transformation matrix for the plane problem, as depicted in Formula (23).

$$R = \begin{bmatrix} R_1 \, 0 \\ 0 \, R_1 \end{bmatrix} \tag{23}$$

where

$$R_1 = \begin{bmatrix} \cos\alpha & -\sin\alpha & 0 \\ \sin\alpha & \cos\alpha & 0 \\ 0 & 0 & 1 \end{bmatrix} \tag{24}$$

In the formula, $\cos\alpha = \frac{x_j - x_k}{l_i}$, $\sin\alpha = \frac{y_j - y_k}{l_i}$, α represents the angles between the length direction of element i and the x-axis of the global coordinate system, while l_i denotes the length of the element.

The coordinate transformation matrix differentiates the node coordinates. It should be noted that the differentiation of the node at which the end of the element is differentiated. As shown in Formulas (25)–(28), it is the differential of each component in the transformation matrix R to the end node j of the element i. The differentiation concerning the starting joint k is similar, and it will not be explicitly outlined here.

$$\frac{\partial \cos\alpha}{\partial x_j} dx_j = \left(\frac{1}{l_i} - \frac{(x_j - x_k)^2}{l_i^3} \right) dx_j \tag{25}$$

$$\frac{\partial \cos\alpha}{\partial y_j} dy_j = \left(-\frac{(x_j - x_k)}{l_i^2} \frac{(y_j - y_k)}{l_i} \right) dy_j \tag{26}$$

$$\frac{\partial \sin\alpha}{\partial x_j} dx_j = \left(-\frac{(y_j - y_k)}{l_i^2} \frac{(x_j - x_k)}{l_i} \right) dx_j \tag{27}$$

$$\frac{\partial \sin\alpha}{\partial y_j} dy_j = \left(\frac{1}{l_i} - \frac{(y_j - y_k)^2}{l_i^3} \right) dy_j \tag{28}$$

By substituting the aforementioned Formulas (25)–(28) into the expression for the transformation matrix, the differential form of the transformation matrix with respect to nodal coordinates can be obtained.

2.4. The Differentiation of the Stiffness Matrix of the Beam Element in the Global Coordinate System

According to Formula (22), the relationship between the stiffness matrix k_i^e of beam element i in the global coordinate system and the stiffness matrix k_i^{*e} in the local coordinate system, the differential of the stiffness matrix of beam element i in the global coordinate system with respect to nodal coordinates x can be obtained, as shown in Formula (29):

$$\frac{\partial {k_i}^e}{\partial x} = \frac{\partial R^T}{\partial x} k_i^{*e} R + R^T \frac{\partial k_i^{*e}}{\partial x} R + R^T k_i^{*e} \frac{\partial R}{\partial x} \tag{29}$$

Then, utilizing the method of assembling finite element stiffness, the differential of the structural total stiffness matrix in the global coordinate system with respect to nodal coordinates can be obtained, as illustrated in Formula (30):

$$\frac{\partial K}{\partial X} = \sum_{i=1}^{NE} \frac{\partial k_i^e}{\partial X} \tag{30}$$

where k_i^e represents the stiffness matrix of element i in the global coordinate system, and NE is the total number of elements in the structure. Subsequently, employing the aforementioned Formulas (10)–(12), the corresponding strain energy gradient can be obtained. The derivation process for the strain energy gradient of spatial beam elements is similar to that of planar beam elements and can be obtained using analogous methods. This will not be expanded in detail here. Once the strain energy gradient is obtained, combined with Formula (4), an iterative process utilizing the gradient method for the nodal coordinates can be employed. This process maintains the grid topology unchanged while seeking an optimized grid layout on the surface, accomplishing grid optimization.

3. Grid Adjustment of Conventional Analytical Surfaces

In typical spherical shells, Kiewitt grid shell exhibits favorable mechanical properties, garnering extensive attention from scholars worldwide [24,25]. This section employs the K6 single-layer spherical grid shell as an example to explore the impact of varying nodal positions on the structural mechanical performance while maintaining the grid topology unchanged. As depicted in Figure 2a, the shell has a span of 30 m, and a rise of 6 m, both with radial and circumferential frequencies set at 6. The members have circular steel tube sections with a diameter of 100 mm and a wall thickness of 4 mm. The load applied is q = 10 kN/m^2, with constraints set as hinged support around the bottom perimeter. Q235 was used and the FEM calculation was based on ANSYS 16.0 software. The static analysis type adopts linear analysis and the load is directly applied to all nodes except for the support nodes. The maximum von Mises stress of the rod is 71 MPa.

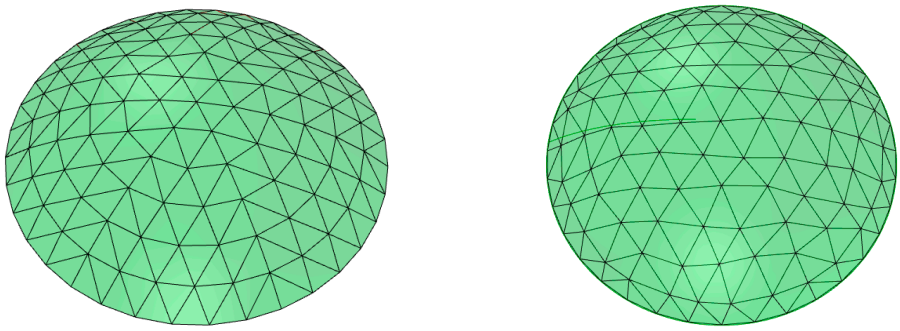

(**a**) K6-type spherical shell (**b**) Adjusted grid

Figure 2. Comparison of the grid before and after adjustment.

As illustrated in Figure 2b, after the optimization, the structural grid has undergone significant changes. The grid tends to cluster toward the edge supports, exhibiting a slight divergence within the internal grid. The lines approximate a parallel distribution along three ribs of the Kiewitt spherical shell, gradually transitioning into a tri-directional grid pattern. The lines become more continuous, facilitating a smoother transmission of forces. This grid layout allows for a more direct transfer of structural loads to the supports. Numerical analysis, as depicted in Figure 3, shows the variation in strain energy. Following the optimization, the structural grid's strain energy was reduced from 3.87 kJ to 3.36 kJ, marking a 13.2% decrease. Regarding the maximum nodal displacement, it decreased from the original 0.73 cm to 0.6 cm, signifying a reduction of 17.8%. Regarding the maximum

stress, it decreased from the original 71 MPa to 66 MPa. This indicates that the adjusted grid has, to a certain extent, enhanced the structural stiffness.

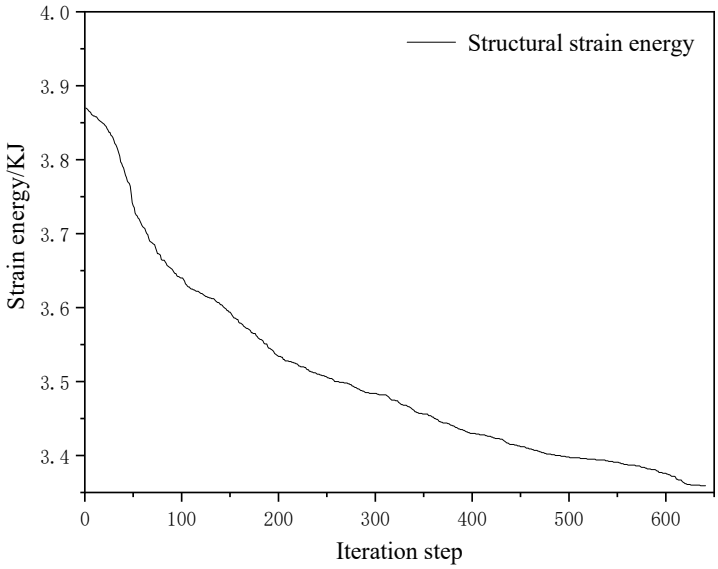

Figure 3. Variation in strain energy.

4. Grid Smoothing

Oftentimes, architectural grids need to possess an aesthetic appeal that highlights the beauty of curves, primarily showcased in the uniformity and smoothness of gridlines. However, after grid adjustment, as depicted in Figure 2b, although the overall strain energy of the structure becomes smaller, the stiffness increases, and the lines become more continuous in topology compared with the initial model, the mesh smoothness is obviously insufficient from the visual point of view, and the mesh is slightly messy, which affects its visual beauty. Therefore, it is necessary to optimize the mesh smoothness after adjustment. In the pursuit of grid smoothing, the Laplacian smoothing method stands out as one of the most typical and commonly used approaches. Its principle is relatively simple, and the algorithm is straightforward to implement. Illustrated in Figure 4, its fundamental principle involves utilizing linear interpolation, where the coordinates of joint i are replaced with the average of coordinates of neighboring joints. This process is expressed through the following computational formula:

$$X_i = \frac{1}{N_i} \sum_{n=1}^{N_i} X_{ni} \tag{31}$$

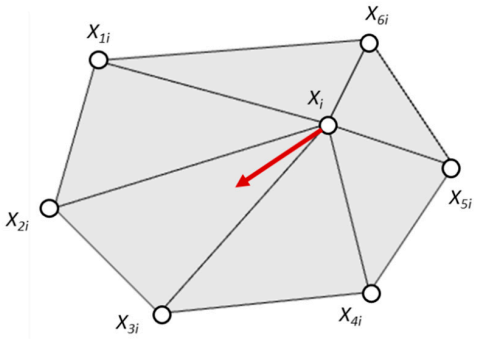

Figure 4. Schematic of the Laplacian grid smoothing principle.

The formula contains variables: X_i represents the coordinate of joint (x_i, y_i, z_i), and N_i and X_{ni} denote the nodal quantity and coordinates of neighboring joints adjacent to joint i, respectively.

Laplacian grid smoothing is practical and efficient, yielding favorable outcomes as long as the initial grid does not contain significant sharp angles. However, it does have a critical flaw: With an increasing number of iterations, the grid gradually contracts. This leads to a deviation between the smoothed grid and the initial one, with a more pronounced deviation occurring with higher iteration counts. As illustrated in Figure 5, the red thin solid lines represent the initial grid, while the green thick solid lines represent the grid after smoothing. As the iteration count increases, the grid becomes more uniformly smoothed. However, the extent of contraction also amplifies significantly deviating from the initial grid.

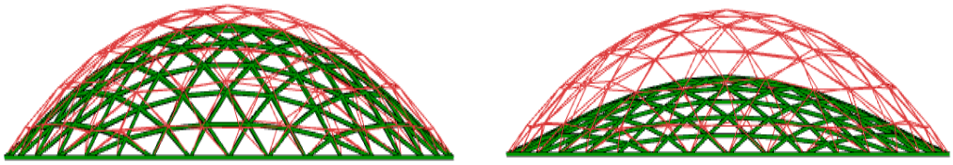

(**a**) step 3 (**b**) step 13

Figure 5. Grid contraction phenomenon.

This paper adopts a relatively simple method to prevent grid contraction. After each grid-smoothing adjustment, the contracted grid is remapped back to the original surface. Given that the deviation between the grid after a single smoothing operation and the original grid is already minimal, remapping the smoothed grid to the surface does not introduce significant errors. This approach effectively meets the requirements of architectural grids, simultaneously smoothing the grid while preventing contraction. Joints along the boundaries remain unchanged and are not adjusted.

Using the aforementioned method to perform grid smoothing on the grid obtained from the strain energy gradient adjustment method, the joints along the boundary lines remain fixed while the internal joints are designated as adjustment points. Each internal joint corresponds to six rods, theoretically achieving an optimal equilateral triangular grid. As depicted in Figure 6, it is the result of grid smoothing. It can be seen that the lines appear noticeably smoother, and the regularity of the grid shape has improved. Upon numerical analysis, the overall strain energy of the smoothed grid structure became 3.43 kJ, approximately 2% higher compared to before smoothing, while the maximum displacement of the structure is at around 0.61 cm and the maximum stress is about 63 MPa. Comparison with the three-directional grid spherical shell, having the same span, aspect ratio, and frequency, shows that even after smoothing, the overall strain energy is still approximately 12% lower, and the maximum displacement is about 20.8% lower compared to the three-directional grid spherical shell. This indicates that after grid smoothing, not only does the geometry of the grid become regular and the lines smoother, but also the structure maintains relatively superior mechanical performance.

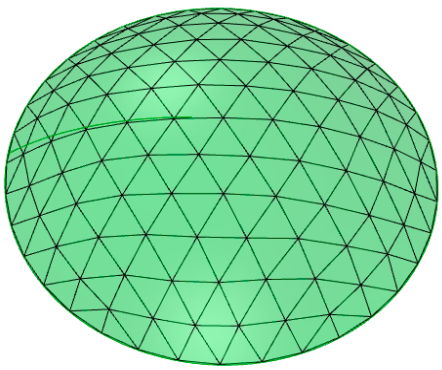

Figure 6. Smoothed grid.

5. Grid Geometric Quality Evaluation Metrics

How to evaluate the quality of a grid has different evaluation criteria in different fields. In the grid division of architectural structures, to consider the aesthetics and economy of the structure, it is usually desired that the divided grid has a regular shape, and the types of grid units should be unified as much as possible. The grid size and the length of the rod are as far as possible to achieve the desired design value.

5.1. Quality of Rod Lengths

The rod is the most basic element of the spatial grid structure, and the length of the rod is directly related to the size of the grid. This paper employs the mean square deviation of rod length $\alpha\prime$, denoted as the parameter, as an indicator for assessing the quality of rod length. For triangular grids, the smaller the mean square deviation of the rod length, the more uniform the grid size.

The mean square deviation of rod length can be expressed as follows:

$$\alpha_l = \sqrt{\frac{\sum (l_i - \bar{l})^2}{n-1}} \tag{32}$$

In the formula, l_i represents the length of the ith rod, $\bar{l}$ denotes the mean length of the rod, and n stands for the number of rods. As it possesses dimensions, the same mean square deviation representing rod uniformity may differ significantly for structures with different grid sizes. Therefore, this paper makes a dimensionless treatment of it and uses the ratio of mean square deviation to the mean length of the rod as the index of the uniformity of the rod length, which is called the equivalent mean square deviation of the rod length, as shown in Formula (33).

$$\alpha\prime = \frac{\alpha_l}{\bar{l}} \tag{33}$$

5.2. Grid Shape Quality

Generally speaking, when dividing the mesh, it is necessary to avoid producing too narrow and long elements. For the triangular mesh, the ideal triangle shape is an equilateral triangle. For reference to the quality criterion of triangular units in the finite element field, the quality evaluation index of triangular units in the building grid can be expressed as follows:

$$\beta = 4\sqrt{3}\frac{S_A}{l_1^2 + l_2^2 + l_3^2} \tag{34}$$

In the formula, S_A is the area of the triangle, and l_1, l_2, l_3 are the lengths of the triangle's sides, respectively.

If all the triangular element shape quality indicators in a grid are taken as a sample $(\beta_1, \beta_2, \beta_3, \cdots\cdots \beta_n)$, where the sample size is denoted as m representing the number of triangular elements in a grid, then the mean of the sample is denoted as $\overline{\beta}$, and the sample variance is denoted as Q.

$$\overline{\beta} = \frac{1}{m}\sum_{i=1}^{m} \beta_i \tag{35}$$

$$Q = \sqrt{\frac{\sum (\beta_i - \overline{\beta})^2}{m-1}} \tag{36}$$

The closer the sample mean is to 1, the better the shape quality of the triangular mesh, and the closer it is to the equilateral triangle, the more regular the mesh shape will be. A smaller sample variance Q implies lesser differences in the quality of triangular grid shapes, indicating more uniformity among the triangular elements in the grid.

5.3. Overall Regularity of the Grid

Considering the grid regularity, for a given grid M, the grid regularity coefficient can be defined as follows:

$$R(M) = \sum_{k=1}^{N} (d_k - D_k)^2 / N = \sum_{k=1}^{N} (d_k^* - 6)^2 / N \quad (37)$$

In the formula, d_k represents the actual value of the joint, D_k stands for the ideal value of the joint, d_k^* indicates the virtual value of the joint, k is the serial number of the joint, and N is the number of joints in the grid. The geometric interpretation of the grid regularity coefficient signifies the deviation between the actual and ideal shapes of the grid, reflecting the degree of regularity. It serves as an indicator to assess the regularity of the grid. If $R(M)$ equals 0, the grid shape is considered regular; otherwise, the larger the $R(M)$ value, the poorer the regularity of the grid. Conversely, a smaller value indicates a more regular shape and better topology.

The calculation of the grid regularity coefficient for the mentioned spherical shell revealed that although the three-way grid spherical shell displays regular only internal grid structures, its edge grid quality is poor. The overall regularity coefficient $R(M)$ is 0.12, whereas, after the smoothing process, the regularity coefficient $R(M)$ drops significantly to 0.047. Consequently, the smoothed grid demonstrates higher quality. Visually, it is apparent that the edge grid of the three-way grid spherical shell is irregular and contains several singular points, as shown in Figure 7. This results in that the force transmission path is not continuous near the boundary, and the force cannot be transmitted more directly to the support, so the structural performance is lower than that of the smoothed mesh.

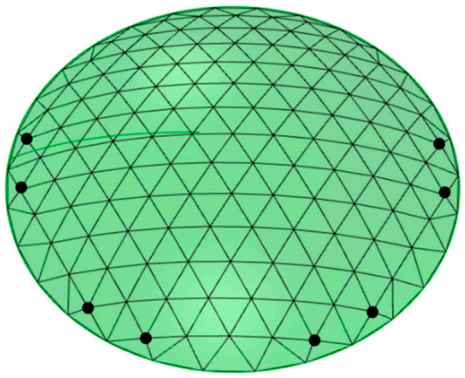

Figure 7. Three-way grid spherical shell.

6. Adjustment of Free-Form Spatial Grid Structure

Through the adjustment of the grid of the Kiewitt spherical shell, the feasibility and effectiveness of the grid optimization method based on strain energy gradient were verified; an improved grid layout with enhanced mechanical performance was obtained. While there exist six typical grid layout forms for spherical shells due to their analytical surfaces and the increasing maturity of spatial structure technology and theory, the meshing scheme of analytical surfaces such as spherical reticulated shells is also becoming more and more perfect. However, for free-form surfaces, their surface forms are different and flexible. So far, there is no general meshing division method. The author of this paper proposed an efficient meshing division method for free-form surfaces based on Coulomb's law [26]. However, its goal is to obtain a uniform mesh layout on the existing surface, and its focus is still limited to geometric objectives. For the divided mesh structure, its mechanical properties are not considered. Therefore, a free-form surface is taken as an example in this paper to discuss the mesh optimization method of a free-form surface based on strain energy gradient.

A free-form surface resembling continuous mountain ranges is shown in Figure 8, with a longitudinal span of 25.6 m, a larger short span of 15.3 m, a minor short span of 6.5 m, a larger sagittal height of 5 m, and a minor sagittal height of 1.9 m. The material parameters

are identical to those of the Kiewitt spherical shell. As depicted in Figure 9, a relatively uniform topological grid is achieved based on geometric objectives. Among these, Grid-a1 represents the grid obtained by the mapping rod adaptive method. Initially, a reasonable topological grid is arranged in the planar domain and then mapped to the spatial surface, followed by adjustments to the rod lengths using the adaptive rod method to achieve a relatively uniform grid topology. Grid-b1 is obtained using the grid generation method based on Coulomb's law and proposed by the authors. Due to the lack of control over the smoothness of grid lines, some singular points appear within the grid interior. However, its grid quality is still good, as shown in Table 1, with a shape quality mean value of 0.97 and a rod length quality of only 0.08.

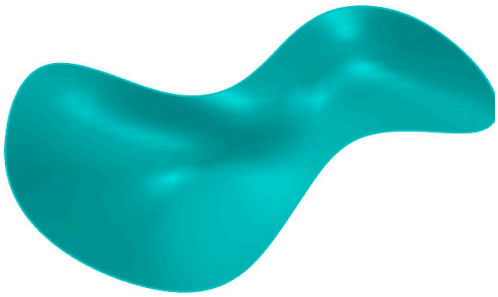

Figure 8. Mountainous terrain surface.

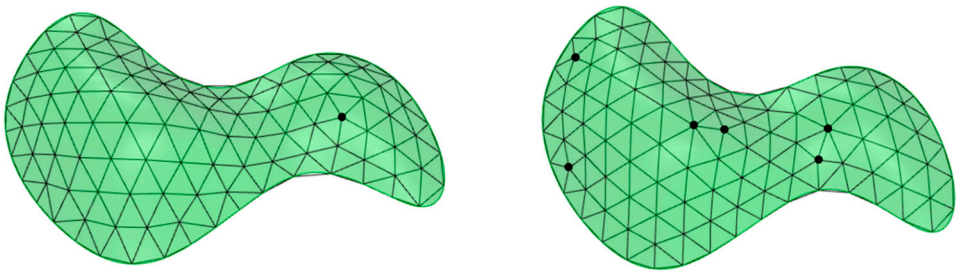

(**a**) Grid-a1 (**b**) Grid-b1

Figure 9. Uniform grid.

Table 1. Performance comparison of different grid layout schemes.

Grid Type	Displacement (cm)	Strain Energy (kJ)	The Mean Value of Shape Quality $\overline{\beta}$	Rod Length Quality α'
Grid-a1	1.16	1.54	0.96	0.12
Grid-a2	0.71	1.16	0.89	0.23
Grid-a3	0.85	1.21	0.94	0.19
Grid-b1	1.13	1.60	0.97	0.08
Grid-b2	0.64	1.12	0.91	0.21
Grid-b3	0.81	1.24	0.94	0.16

Targeting structural strain energy, adjustments were made separately to the Grid-a1 and Grid-b1 grids, resulting in the grid configurations Grid-a2 and Grid-b2 as shown in Figure 10. It is noticeable that the uniformity of the grids deteriorated: The grids became sparse at the mountain peaks and displayed a contraction trend in the valleys, with lines becoming elongated. Both grids exhibited a similar trend in sparseness. Analyzing their grid quality, the shape quality of the grids decreased by approximately 7%, which is not significant. However, the equivalent rod length means square deviation decreased significantly, indicating poorer grid uniformity. Analyzing their mechanical performance, it was observed that after grid adjustments, the maximum nodal displacement in Grid-a1 decreased by 38.8%, and the structural strain energy decreased by 24.7%. In Grid-b2, the maximum nodal displacement decreased by 43.3%, and the structural strain energy

decreased by 30%. This suggests that although the geometric indicators declined after adjusting the uniform grid, its mechanical performance significantly improved.

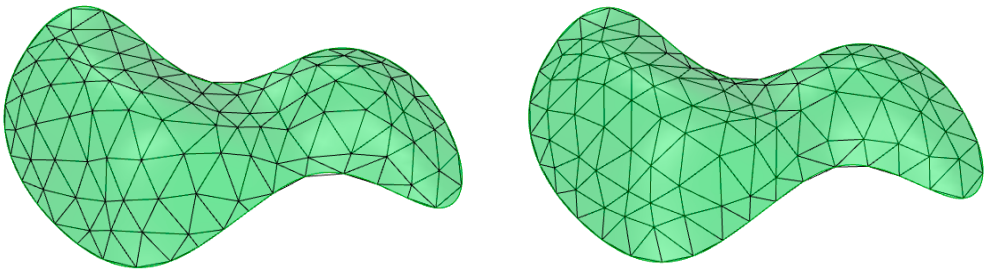

(**a**) Grid-a2 (**b**) Grid-b2

Figure 10. Adjusted grids.

To balance both geometric and mechanical criteria, the adjusted grids Grid-a2 and Grid-b2 were smoothed individually, resulting in corresponding grids Grid-a3 and Grid-b3, as shown in Figure 11. Visually, the smoothed grids appear relatively regular in shape, with smoother lines, and an overall sparse with regularity. Numerically, as shown in Table 1, the quality indicators for shape and rod length have improved compared to the adjusted grids. Both types of grids show a shape quality mean value of over 0.94, while the rod length quality remains below 0.19, indicating acceptable geometric properties. Concerning structural mechanical performance, the overall strain energy slightly increased after smoothing for both grids, yet still reduced compared to the initial uniform grid, at 78.57% and 77.50%, respectively. Additionally, the maximum nodal displacement decreased by 26.7% and 28.3%, respectively, compared to the initial grid. This suggests that grid layouts predominantly focused on geometric objectives have room for improvement in terms of mechanical performance.

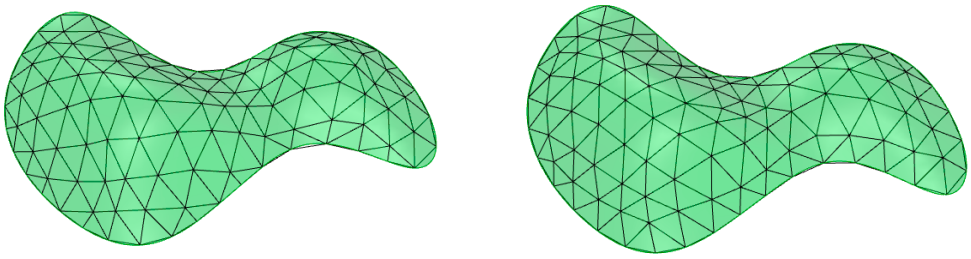

(**a**) Grid-a3 (**b**) Grid-b3

Figure 11. Smoothed grids.

7. Conclusions

To improve the static performance of the free-form surface spatial grid structure, while ensuring the uniformity of its structural grid and not reducing the grid quality, a free-form surface grid optimization method is proposed in this paper based on the strain energy gradient. The gradient of the overall strain energy of the structure to the nodal coordinates is first derived. Then, based on the sensitivity of the overall strain energy of the structure to the change of the nodal coordinates, the overall strain energy of the structure is taken as the target. The architectural surface is the constraint to adjust the nodal coordinates, complete the grid optimization, and obtain the grid topology with the largest stiffness.

Finally, some results are as follows:

1. The final grid layout obtained using the optimization method proposed in this paper, the overall strain energy is reduced, and the overall stiffness of the structure is increased, which indicates that the static performance of the optimized structure is improved. In the example of a conventional spherical surface, the strain energy of the structure obtained by this method is 13.2% lower than that of the initial structure, and the maximum nodal displacement of the structure is 17.8% lower than that of the initial structure.

2. In the example of a free-form surface spatial grid structure, compared with the initial structure, the overall strain energy of the grid structure obtained by the method proposed in this paper is reduced by more than 25%, and the maximum nodal displacement is reduced by more than 38%, which shows the effectiveness of this method for a free-form surface structure.
3. The static performance of the grid obtained by the method proposed in this paper has been improved, but its grid quality has declined, and the grid smoothness is slightly insufficient. Furthermore, after the Laplacian grid smoothing, the grid quality is effectively improved, and the static performance of the structure does not change much. Compared with the initial grid, the strain energy of the grid structure after smoothing is reduced by about 22%, and the maximum nodal displacement is reduced by about 25%.

Author Contributions: Conceptualization, F.L. and K.D.T.; methodology, F.L.; software, T.X.; validation, T.X. and Y.W.S.C.; formal analysis, T.X.; writing—original draft preparation, T.X.; writing—review and editing, K.D.T.; visualization, Y.W.S.C.; supervision, F.L.; project administration, F.L.; funding acquisition, F.L. All authors have read and agreed to the published version of the manuscript.

Funding: This research was funded by the Natural Science Foundation of China (Grant No: 52308213); the Natural Science Foundation of Jiangsu Province, China (Grant No: BK20220593); the China Postdoctoral Science Foundation (Grant No: 2023M740582); Jiangsu Province Higher Education Basic Science (Natural Science) Research Project (Grant No: 22KJB560033).

Data Availability Statement: The original contributions presented in the study are included in the article, further inquiries can be directed to the corresponding author.

Conflicts of Interest: The authors declare no conflicts of interest.

References

1. Frey, P.J. 3D Delaunay grid generation coupled with an advancing-front approach. *Comput. Methods Appl. Mech. Eng.* **1998**, *157*, 115–131. [CrossRef]
2. Cen, P.C. Parameter Surface Description and Meshing Algorithm of Spatial Structure. Ph.D. Thesis, Zhejiang University, Hang Zhou, China, 2006.
3. Ding, H.; Luo, Y.Z. Isoparametric line segmentation method for grid generation of free form reticulated shell structure. *J. Zhejiang Univ. (Eng. Sci.)* **2014**, *48*, 1795–1801.
4. Wei, D.J.; Shu, G.P. Free form surface grid partition and optimization method. *Build. Struct.* **2013**, *19*, 48–53.
5. Gao, B.; Hao, C.; Li, T.; Ye, J. Grid generation on free-form surface using guide line advancing and surface flattening method. *Adv. Eng. Softw.* **2017**, *110*, 98–109. [CrossRef]
6. Pan, W.; Wu, H.; Li, T.; Gao, B. Free form surface meshing based on surface expansion. *J. Zhejiang Univ. (Eng. Sci.)* **2016**, *50*, 1973–1979.
7. Cuilliere, J.C. An adaptive method for the automatic triangulation of 3D parametric surfaces. *Comput.-Aided Des.* **1998**, *30*, 139–149. [CrossRef]
8. Zheleznyakova, A.L. Molecular dynamics-based triangulation algorithm of free-form parametric surfaces for computer-aided engineering. *Comput. Phys. Commun.* **2015**, *190*, 1–14. [CrossRef]
9. Zheleznyakova, A.L.; Surzhikov, S.T. Molecular dynamics-based unstructured grid generation method for aerodynamic applications. *Comput. Phys. Commun.* **2013**, *184*, 2711–2727. [CrossRef]
10. Pottmann, H. Geometry and New and Future Spatial Patterns. *Archit. Des.* **2009**, *29*, 60–65. [CrossRef]
11. Shepherd, P.; Richens, P. The case for subdivision surfaces in building design. *J. Int. Assoc. Shell Spat. Struct.* **2012**, *53*, 237–245.
12. Schlaich, J.; Schober, H.; Kürschner, K. New Trade Fair in Milan—Grid Topology and Structural Behaviour of a Free-Formed Glass-Covered Surface. *Int. J. Space Struct.* **2005**, *20*, 1–14. [CrossRef]
13. Bouhaya, L.; Baverel, O.; Caron, J. Optimisation Structurelle des Gridshells. Ph.D. Thesis, Université Paris-Est, Paris, France, 2010.
14. Lefevre, B.; Douthe, C.; Baverel, O. Buckling of elastic grid shells. *J. Int. Assoc. Shell Spat. Struct.* **2015**, *56*, 153–171.
15. Shimada, K.; Gossard, D.C. Automatic triangular grid generation of trimmed parametric surfaces for finite element analysis. *Comput. Aided Geom. Des.* **1998**, *15*, 199–222. [CrossRef]
16. Zhou, Y.; Nie, Y.; Zhang, W. A modified bubble placement method and its application in solving elliptic problem with discontinuous coefficients adaptively. *Int. J. Comput. Math.* **2017**, *94*, 1268–1289. [CrossRef]
17. Wang, Q.S.; Ye, J.; Wu, H.; Gao, B.Q.; Shepherd, P. A triangular grid generation and optimization framework for the design of free-form grid shells. *Comput. Aided Des.* **2019**, *113*, 96–113. [CrossRef]

18. Pottmann, H.; Jiang, C.; Höbinger, M.; Wang, J.; Bompas, P.; Wallner, J. Cell packing structures. *Comput.-Aided Des.* **2015**, *60*, 70–83. [CrossRef]
19. Su, L.; Zhu, S.L.; Xiao, N.; Gao, B.Q. An automatic grid generation approach over free-form surface for architectural design. *J. Cent. South Univ.* **2014**, *21*, 2444–2453. [CrossRef]
20. Shan, Z.; Chen, L.; Wang, Q.; Wu, H.; Gao, B. Simplified quadrilateral grid generation of complex free-form gridshells by surface fitting. *J. Build. Eng.* **2022**, *48*, 103827. [CrossRef]
21. Zhang, X. Grid mesh and Optimization of Single-Layer Free-form Rigid Structure and Practical Applications. Ph.D. Thesis, Chongqing University, Chongqing, China, 2015.
22. Allen, E.; Zalewski, W. *Form and Forces: Designing Efficient, Expressive Structures*; John Wiley & Sons, Inc.: Hoboken, NJ, USA, 2009.
23. Fujita, S.; Ohsaki, M. Shape Optimization of Free-form Shells Considering Strain Energy and Algebraic Invariants of Parametric Surface. In Proceeding of IASS, Valencia, Spain, 28 September–2 October 2009; pp. 525–535.
24. Ye, J.; Zhu, N. Redundancy of single-layer dome under earthquake action based on response sensitivity. *Int. J. Steel Struct.* **2016**, *16*, 125–138. [CrossRef]
25. Zhu, N.; Ye, J. Structural Vulnerability of a Single-Layer Dome Based on Its Form. *J. Eng. Mech.* **2014**, *140*, 112–127.
26. Liu, F.; Feng, R. Automatic triangular grid generation on a free-form surface using a particle self-organizing system. *Eng. Comput.* **2019**, *36*, 377–389. [CrossRef]